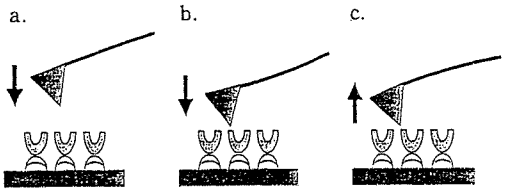

図2 AFM探針の試料の相互作用と板ばねのそり
a: 試料へ接近. b: 試料へ接触と, 板ばねのそり.
c: 試料からの離脱と原子間力による板ばねのそり.

る(図2). 試料表面にナノメーターレベルの距離で接近した板ばねは探針と試料との間に生じる原子間力に応じてそり(deflection)などの変位を起こす. そこにレーザー光を照射し, 生じる反射光を四分割フォトダイオードディテクターで検出し, その結果に基づきサンプルのトポグラフィカルな情報を画像化するのである. 具体的な蛋白質のイメージングの例は, 4. 測定法の項に後述する.

b. アンフォールディング

蛋白質の機能に大きくかかわる三次元構造は, 蛋白質のフォールディング(折りたたみ)により形成されるが, その機構に関しては未知の部分が多い. しかし, BSEに代表されるように蛋白質のミスフォールディングが疾患に関連している例が知られるようになり, フォールディングに関する基礎的知見は, 疾患の検出あるいは診断に重要な役割を果たすことが期待される.

ミュンヘン大学のGaubらのグループは, 膜貫通型蛋白質の一つバクテリオロドプシンを用いて, AFMによるアンフォールディングの実験を行った[3]. バクテリオロドプシン分子が多量に発現した*Halobacterium salinarum*の紫膜を劈開したばかりのマイカ表面上にマウントし, そこへAFM探針を接触させた後引っぱり上げると, フォースカーブに繰り返しパターンがみられた(図3). フォースカーブ上にピークが生じた距離と, フォールディングしているアミノ酸残基の長さは一致しており, ピークは蛋白質のフォールディングパターンを示していると考えられた.

c. 分子間相互作用の測定
(chemical force microscopy)

ハーバード大学のLieberらは, AFM探針先端を特定の有機化合物で修飾し, 対象とする試料表面の官能基を選択的に検出しようとするchemical force microscopyを報告した[4]. 彼らは, 金で表面をコートしたシリコンナイトライド探針上に親水基(-COOH)あるいは疎水基($-CH_3$)を末端に有するアルキルチオール分子で自己組織化膜(self assembled monolayer: SAM)を形成させる方法でAFM探針の修飾を行い, フォースカーブ測定を行った(図4). その結果, CH_3/CH_3, CH_3/COOHおよびCOOH/COOH対での相互作用の違いをフォースカーブで検出することに成功した.

同様に, SAMで修飾したAFM探針を用いて, 分子のキラリティーの判別[5], 超分子ホストゲストコンプレックスの結合能の測定[6]などが報告されている. Gaubらのグループは, このchemical force microscopyをレセプター対リガンドの結合能測定に応用し, ストレプトアビジンとビオチンの結合能をフォースカーブとして測定した. この手法を種々のレセプター-リガンド対に応用することで, 将来的にはごく微量の蛋白質を用いたドラッグスクリーニング法として有用となる可能性も考えられる(図5).

4. 測定法(各論)

a. 試料の調製法

AFM測定において, 最も要となるところが, 試料の調製法である. 測定結果の良し悪しは, この試料調製法によるといっても過言でない. AFMは基本的にナノメーターレベルでの表面解析である. したがって, 測定する試料はできるだけ平坦なものである必要がある. 調製した試料の凸凹が激しいと, 単分子レベルでの測定を行う解像度が望めなくなるからである.

基板としては, マイカ, 単結晶金, グラファイトなどの原子レベルで平坦なものを用いる. マイカ, グラファイトは, 劈開したばかりのものを用い, 金は蒸着後高温でアニールし単結晶表面を形成したものを用いる. ここに目的の蛋

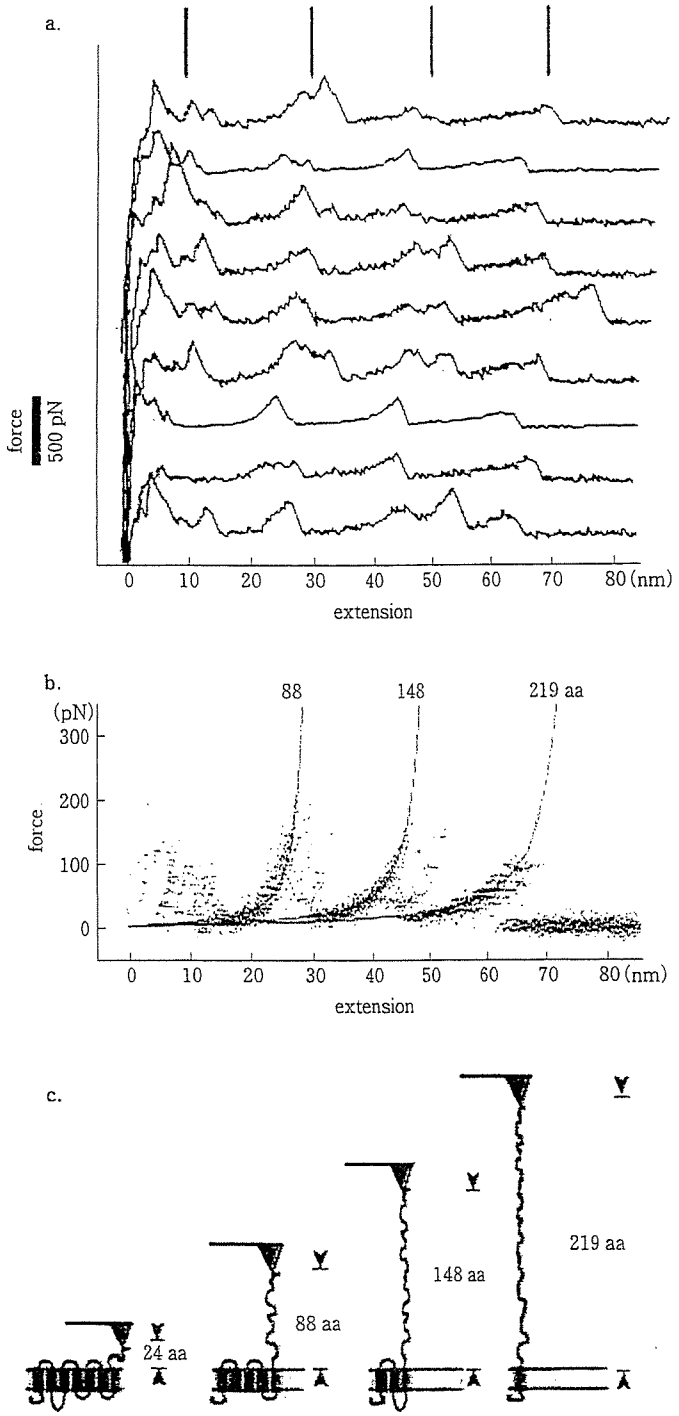

図3　AFMを用いた蛋白質アンフォールディングの実験

細胞膜中の膜蛋白質にAFM探針を接触(−1nN，1秒間)させ，C末端をAFM探針の先端に接着させる．それを引っ張ると，フォースカーブが生じ，カーブ上のピークまでの距離は，予測されているフォールディングパターンのアミノ酸残基の長さと一致する．

(文献[3]より引用)

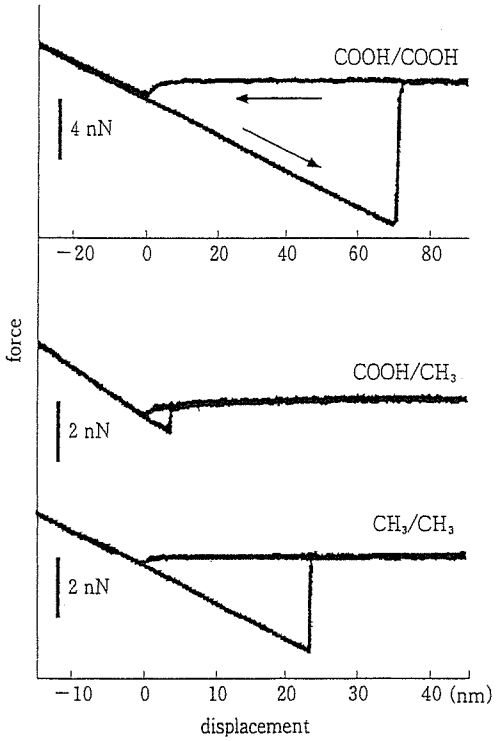

図 4 末端に親水基あるいは疎水基を有する分子の自己組織化膜で修飾した AFM 探針によるフォースカーブの測定
(文献[4]より引用)

白質を単分子膜として不動化させる．測定する蛋白質は，native なものを用いる場合もあれば，精製したものを用いる場合もある．膜結合型蛋白質では，細胞膜上に蛋白質が大量に発現していれば，それを直接測定することも可能であるが，精製した蛋白質を基板上に不動化したうえで測定する場合もある．測定は，溶媒を乾燥させたうえで行う場合と，溶液中でそのまま行う場合がある．いずれにしても超純粋な溶媒を用い，ほこりなどが基板に吸着しないような環境下で試料調製を行う必要がある．図 6 に調製法の異なる試料のイメージングの例を示す．乾燥した試料の大気中測定では蛋白質の凝集がみられたが，水溶液中での測定では，分散した蛋白質が単分子レベルで観測された．緩衝溶液中での測定では，蛋白質の再構築がよく観察され，チャネル孔らしき構造も観測された[7]．

b. 測　定

1) 測定モード

基本測定モードには，コンタクトモード，タッピングモード，ノンコンタクトモードの 3 種類があり(図 7)，測定する試料に応じてモードを選択する必要がある．コンタクトモードは，探針の先端と試料を接触させながら測定する方法で，探針と試料の接触により生じる板ばねのそりをフィードバックシステムで一定に保つように設定し，電気的信号をもとに画像化する．スキャン速度を上げることができる，比較的凹凸の大きい試料の測定にも適しているなどの利点があるが，直接接触することにより試料に損傷が生じる可能性があるため，ソフトな試料(特に生物学的試料)の測定にはあまり適していない．これに対し，タッピングモードと，ノンコンタクトモードは一定の周波数で振動させた板ばねを用いた測定法である．タッピングモードでは，探針が試料に最も近づくときに軽く試料に接触するが，ノンコンタクトモードでは，全く接触しない．試料と探針が接近すると，相互作用により振動幅に変化が生じるが，これらのモードではフィードバックシステムにより振動幅を一定に保つよう調節し，その調節に必要な電気的信号をもとに画像化を行う．双方とも試料と探針の接触が少なく，ソフトな試料の測定に適している．

2) カンチレバー

AFM の解像度は探針の先端に依存する．すなわち，高分解能な測定のためには，探針の先端がなるべく微細であることが重要である．この微細加工が可能であること，更に，高い共振周波数を得られるという理由から，シリコン，シリコンナイトライドなどの素材が現在汎用されている．また，前述の chemical force microscopy などの応用測定に用いられる，金コート済みの探針も市販されている．

更に高い解像度を達成するためには，探針の先端が非常に鋭利であることが求められ，単分子であることが理想である．より微細な探針素材としてはカーボンナノチューブを用いる研究も行われている[8]．

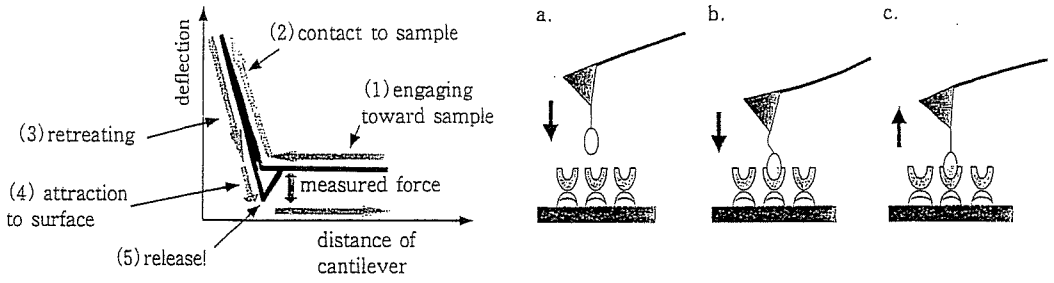

図5 Chemical force spectroscopy を用いたレセプターとリガンド間の分子間相互作用の実験
a: 試料に接近. b: 試料に接触. c: 相互作用(フォースとして現れる).

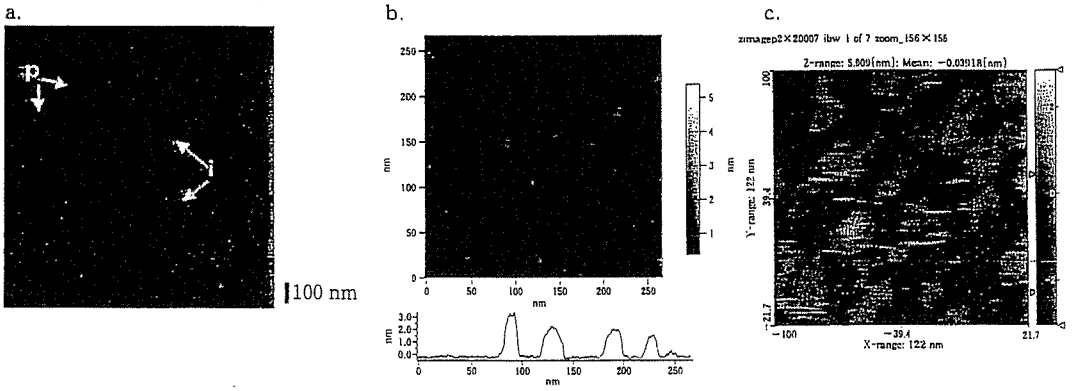

図6 膜蛋白質 $P2X_2$ 受容体の AFM によるイメージング
a: 蛋白質水溶液をマイカ上に滴下後, 乾燥させたサンプルを測定した画像. 蛋白質が島状に凝集している状態が見える.
b: 蛋白質水溶液をマイカ上に滴下, そのまま水中で測定した画像とその断面図. 蛋白質が単分子状に分散している状態が見える.
c: 蛋白質の緩衝溶液をマイカ上に滴下, そのまま緩衝液中で測定した画像. 蛋白質が再構築し, チャネル状の構造を取っている状態が見える.

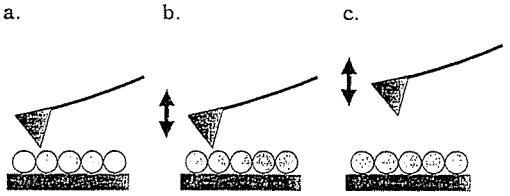

図7 AFM の測定モード
a: コンタクトモード. b: タッピングモード.
c: ノンコンタクトモード.

3) 膜結合型蛋白質のイメージングの例

難溶性で単結晶の作成が難しい膜蛋白質のイメージングにおいて, AFM が最も威力を発揮する. ドレスデン工科大学の Müller らの研究グループは, 膜蛋白質の AFM イメージングを精力的に行っている. その成果の例を図8に示す.

図8は, Cx26 Hela 細胞に多量に発現したコネキシン26分子を精製後, マイカ上にマウントして緩衝液中で AFM 測定を行ったものである[9]. コネキシン分子の細胞外部分がサブ分子レベルで観測されている. コネキシン分子が六量体でチャネル孔を有する様子がわかる. 図8-aはカルシウムイオン非存在下, bは存在下での測定で, カルシウムイオンの添加により蛋白質のコンフォーメーションが変化し, チャネルの入り口の直径が1.5 nm から 0.6 nm へと小さくなることが観測された.

図9は脂質二重膜中に埋包させた膜蛋白質

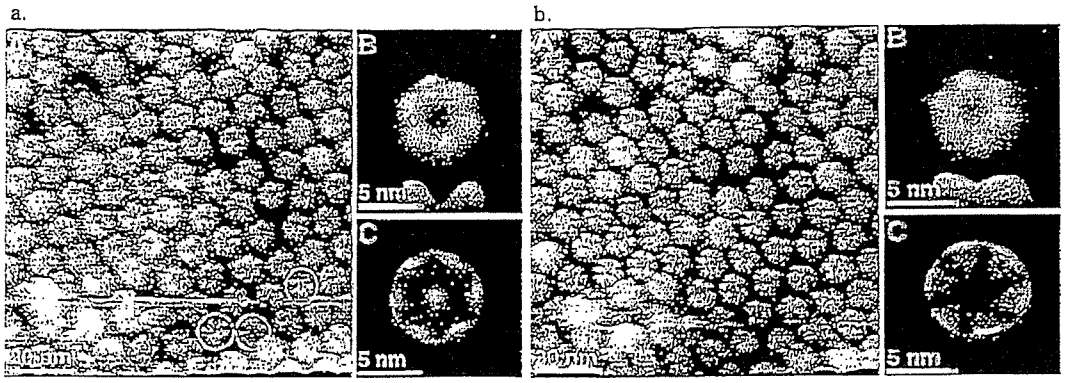

図 8 コネキシン分子の AFM イメージ
a: Ca^{2+}非存在下での画像. b: Ca^{2+}存在下での画像. コンフォーメーションの変化がみられる.
(文献[9]より引用)

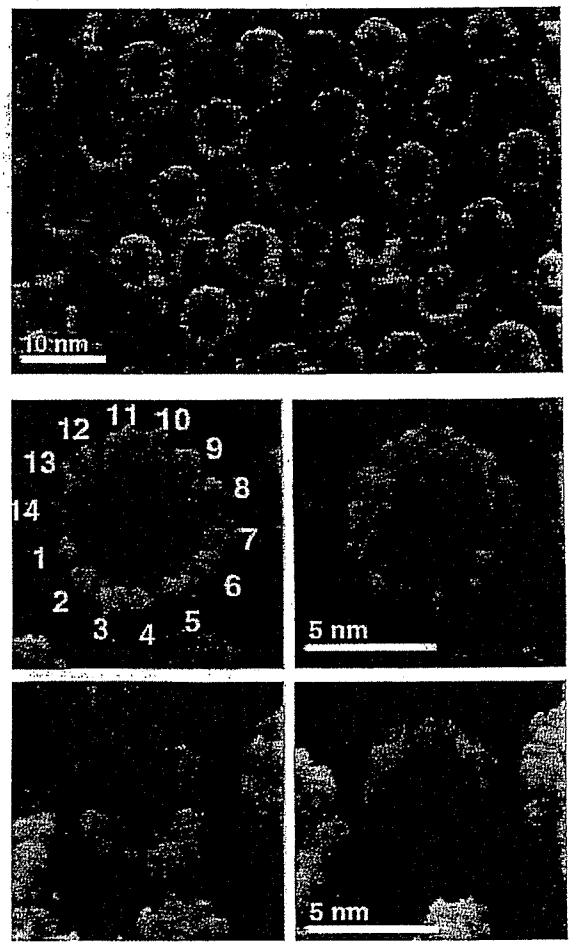

図 9 精製後脂質二重膜中で再構築させた spinach chloroplast ATP synthase の AFM イメージ
(文献[10]より引用)

のAFMイメージの例である[10,11]. 精製したATP synthaseをdodecyl maltosideの存在下，フォスファチジルコリンおよびフォスファチジン酸と混合することで埋包させマイカ上で測定を行った.

5. 今後の進展

以上に紹介したように，AFMの生物試料への応用は主として膜蛋白質の解析に利用されている．これは，膜蛋白質の基板上での配向が均一であり，解析が行いやすいためである．膜蛋白質のX線結晶構造解析が酵素などの水溶性蛋白質より困難であることを考慮すれば，解像度は落ちるとはいえAFMの形状解析がこの種の蛋白質の研究に今後も有用であると予想される．また，X線による構造解析が既になされている蛋白質についても，AFMによる水溶液中の形状解析が動的構造について新たな知見をもたらす可能性が考えられる.

本稿では，単一蛋白質のイメージングの例を紹介したが，2種以上の蛋白質の水溶液中での会合状態を観察することも可能である．例えば，受容体とこれに直接的に働くエフェクター分子(G蛋白質など)との会合状態を観察することにより，生化学的応答の機構の可視化が可能となるかもしれない.

分子間相互作用の測定については，受容体とそのリガンド，酵素とその基質などの分子相互作用を1分子レベルで解析できれば，生体の分子メカニズムについて，これを力学的に解析するという全く新しい分野を切り開くことになるであろう.

文　献

1) Binning G, et al: Atomic force microscope. Phys Rev Lett **56**: 930-934, 1986.
2) Binning G, et al: Surface study by scanning tunneling microscopy. Phys Rev Lett **49**: 57-61, 1982.
3) Oesterhelt F, et al: Unfolding pathways of individual bacteriorhodopsins. Science **288**: 143-146, 2000.
4) Frisbie CD, et al: Functional group imaging by chemical force microscopy. Science **265**: 2071-2074, 1994.
5) McKendry R, et al: Chiral discrimination by chemical force microscopy. Nature **391**: 566-568, 1998.
6) Schönherr H, et al: Individual supramolecular host-guest interactions studied by dynamic single molecule force spectroscopy. J Am Chem Soc **122**: 4963-4967, 2000.
7) Nakazawa K, et al: Purification and aqueous phase atomic force microscopic observation of recombinant P2X2 receptor. Eur J Pharmacol **518**: 107-110, 2005.
8) Wooley AT, et al: Structural biology with carbon nanotube AFM probes. Chem Biol **7**: R193-R204, 2000.
9) Müller DJ, et al: Conformational changes in surface structure of isolated connexin 26 gap junctions. EMBO J **21**: 3598-3607, 2002.
10) Seelert H, et al: Proton-powered turbine of a plant motor. Nature **405**: 418-419, 2000.
11) Seelert H, et al: Fourteen protomers compose the oligomer III of the proton-rotor in spinach chloroplast ATP synthase. J Mol Biol **333**: 337-344, 2003.

ARTICLE IN PRESS

Available online at www.sciencedirect.com

ScienceDirect

Toxicology in Vitro xxx (2006) xxx–xxx

Toxicology in Vitro

www.elsevier.com/locate/toxinvit

Two-dimensional electrophoresis of protein from cultured postimplantation rat embryos for developmental toxicity studies

Makoto Usami [a,*], Katsuyoshi Mitsunaga [b], Ken Nakazawa [a]

[a] *Division of Pharmacology, National Institute of Health Sciences, 1-18-1, Kamiyoga, Setagaya, Tokyo 158-8501, Japan*
[b] *School of Pharmaceutical Sciences, Toho University, Japan*

Received 6 January 2006; accepted 10 November 2006

Abstract

A simple method for two-dimensional electrophoresis (2-DE) of rat embryonic protein was described. Rat embryos cultured for 24 h from day 10.5 of gestation were used as protein samples. Protein samples were lysed in rehydration buffer and separated by isoelectric focusing with immobilized pH gradient for the first dimension and by sodium dodecyl sulfate–polyacrylamide gel electrophoresis for the second dimension. The use of the DeStreak Reagent as an antioxidant in the lysis buffer and electrode pads in the isoelectric focusing greatly improved the 2-DE pattern. When an embryo was used as a protein sample, about 800 protein spots were detected by silver staining in a 2-DE gel of the standard format. Eighty-one protein spots were identified by mass spectrometry for a primary 2-DE map. The same method could be applied to yolk sac membranes from the cultured embryos. The present method was considered to be suitable for a concomitant 2-DE analysis in in vitro developmental toxicity studies.

Keywords: Two-dimensional electrophoresis; Rat; Embryo; Yolk sac; Developmental toxicity; Proteome

1. Introduction

Recent advances in two-dimensional electrophoresis (2-DE) made it possible to analyze the changes in protein expression pattern caused by exogenous stimulations in various tissues, such as the liver (Fountoulakis et al., 2000), kidney (Xu et al., 2005) and blood components (Piubelli et al., 2005). In developmental toxicity studies, the analysis of embryonic protein expression pattern by 2-DE is considered to be useful for the mechanism-based evaluation of developmental toxicants.

On the other hand, it is expected that the cultured rat embryos can be better protein samples for the analysis of protein expression pattern in developmental toxicity studies. Postimplantation rat embryo culture is now widely used in developmental toxicity studies, by which embryos can be exposed to test chemicals under controlled conditions with a small number of animals and a small amount of test chemicals (Schmid et al., 1997).

However, there have been no suitable 2-DE methods for the analysis of embryonic protein expression pattern since most methods are for radio-labeled proteins but not for total proteins (Baumgartner et al., 1994; Praxmayer et al., 1992). The standard 2-DE methods that we tried could not be applicable because of a high salt concentration and poor solubility of embryonic samples. A method reported for the proteome analysis of mouse embryos is not considered suitable for routine analysis in developmental toxicity studies because of troublesome pretreatment of embryo samples, i.e., water-wash and dry-ice freezing (Greene et al., 2002).

In the present study, we described a simple 2-DE method for the analysis of cultured postimplantation rat embryos. By our method about 800 protein spots were detected in a

Abbreviations: 2-DE, two-dimensional electrophoresis; IEF, isoelectric focusing; IPG, immobilized pH gradient; SDS, sodium dodecyl sulfate; PAGE, polyacrylamide gel electrophoresis.

* Corresponding author. Tel.: +81 3 3700 1141x342; fax: +81 3 3707 6950.
E-mail address: usami@nihs.go.jp (M. Usami).

0887-2333/$ - see front matter © 2006 Elsevier Ltd. All rights reserved.
doi:10.1016/j.tiv.2006.11.003

Please cite this article in press as: Usami, M. et al., Two-dimensional electrophoresis of protein from cultured postimplantation rat embryos for developmental toxicity studies, Toxicol. In Vitro (2006), doi:10.1016/j.tiv.2006.11.003

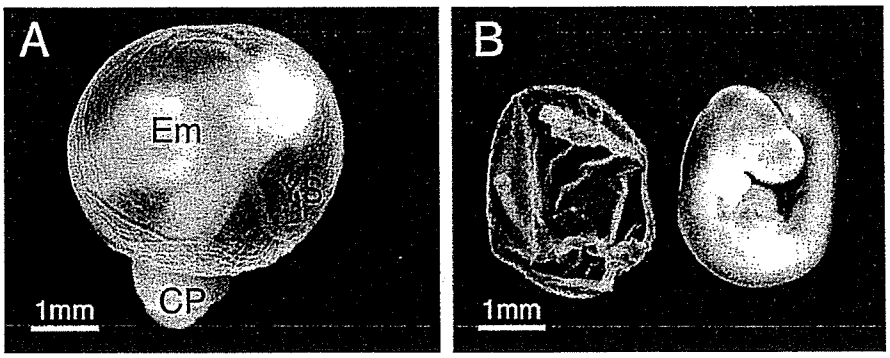

Fig. 1. Appearance of a rat embryo cultured for 24 h from day 10.5 of gestation: (A) At the end of culture. Em, embryo; YS, yolk sac; CP, chorio-allantoic placenta. (B) After the separation of embryonic membranes. Left: yolk sac membrane, Right: embryo.

single gel. The protein spots were identified by mass spectrometry for the construction of a primary 2-DE map of cultured postimplantation rat embryos. The same method could be applied to the 2-DE analysis of yolk sac membranes.

2. Materials and methods

2.1. Embryo culture

Rat embryos were cultured for 24 h by the roller bottle method as previously described (Usami and Ohno, 1996). Embryos were explanted from pregnant Wistar rats (Crlj: WI, Charles River Laboratories Japan, Inc., Kanagawa, Japan) at day 10.5 of gestation (plug day = day 0.5) under ether anesthesia. Explanted embryos were placed in a culture bottle at one embryo per 0.8–1 ml of rat serum and rotated at 35 rpm for 24 h at 37–38 °C. After the culture, the embryos and yolk sac membranes were washed three times with ice-cold buffer (0.01 M Tris–HCl, pH 7.0, 0.15 M NaCl), and placed in 1.5-ml eppendorf tubes individually with a minimum amount of the buffer for storage at −80 °C.

2.2. Preparation of embryo or yolk sac membrane samples

For 2-DE, frozen embryos or yolk sac membranes were lysed in 300 μl of rehydration buffer consisting of 7 M urea, 2 M thiourea, 2% (w/v) CHAPS, 2% (w/v) SB-10, 0.5% (v/v) IPG buffer (Amersham Biosciences, Piscataway, NJ) and 0.12% (v/v) DeStreak Reagent (Amersham Biosciences), by pulsed sonication with a 7-mm ∅ tip immediately after the addition of the buffer. Care was taken to avoid heating and forming during the sonication. Embryo or yolk sac membrane lysates were kept at 20 °C and their protein concentration was determinded with the 2D Quant Kit (Amersham Biosciences).

2.3. Isoelectric focusing (IEF) for the first dimension of 2-DE

IEF was carried out on 13-cm immobilized pH gradient (IPG) strips (Immobiline DryStrip pH 3–10 NL, Amersham Biosciences) with the IPGphor system (Amersham Biosciences). IPG strips were rehydrated with the rehydration buffer containing 50 μg protein of embryo or yolk sac membrane lysate for at least 12 h at 20 °C under a cover with silicon oil. Before the start of IEF, 3-mm-wide IEF electrode strips (Amersham Biosciences) damped were inserted between the IPG strip and both electrodes as electrode pads. Electrophoresis conditions were – Step 1: Step-*n*-hold at 500 V for 1 h, Step 2: Gradient at 1000 V for 1 h, Step 3: Gradient 8000 V for 2.5 h with the current limit of 50 μA per IPG strip. When electrophoresis for the second dimension was not carried out immediately after IEF, the IPG strips were stored at −80 °C.

2.4. Sodium dodecyl sulfate–polyacrylamide gel electrophoresis (SDS–PAGE) for the second dimension of 2-DE

SDS–PAGE was performed according to the method of Laemmli (Laemmli, 1970) except that no stacking gel was used. After IEF, IPG strips were equilibrated with 5 ml of SDS equilibration buffer consisting of 0.05 M Tris–HCl, pH 8.8, 6 M urea, 30% (v/v) glycerol, 2% (w/v) SDS, 0.025% (w/v) bromophenol blue. For the first equilibration, IPG strips were placed in a tube containing equilibration buffer with dithiothreitol (50 mg/5 ml) and rocked for 20 min. For the second equilibration, IPG strips were placed in a tube containing equilibration buffer with iodoacetamide (125 mg/5 ml) and rocked for 20 min. Equilibrated IPG strips were applied onto polyacrylamide gels (12.5% T, 2.6% C, 14 × 6 cm) and sealed with 0.5% agarose in electrode buffer. Electrophoresis was carried at a constant current of 10 mA

Table 1
Size and protein content of cultured rat embryos

Item	Mean	Standard deviation
Yolk sac diameter (mm)	4.37	0.10
Crown-rump length (mm)	3.99	0.16
Number of somite pairs	26.0	0.67
Embryo protein (μg)	298.2	31.0
Yolk sac protein (μg)	153.0	20.2

Values for 10 embryos are shown.

Please cite this article in press as: Usami, M. et al., Two-dimensional electrophoresis of protein from cultured postimplantation rat embryos for developmental toxicity studies, Toxicol. In Vitro (2006), doi:10.1016/j.tiv.2006.11.003

per gel for 15 min and thereafter 20 mA per gel until the dye front reached the edge of the gel.

2.5. Stain of 2-DE gel and protein identification

After SDS–PAGE, 2-DE gels were stained with the Plus One Silver Staining Kit Protein (Amersham Biosciences) using the Multi Processor (Amersham Biosciences) according to the manufacturer's instruction. Stained 2-DE gels were scanned and analyzed with the PD Quest 2D analysis software (Bio-Rad, Hercules, CA).

For the identification of protein spots by mass spectrometry, 2-DE gels were stained with the mass-analysis compatible Proteo Silver staining kit (Sigma, St. Louis, MO) and protein spots were excised and cut into 1-mm cubes with a scalpel. Proteins in the gel cubes were digested with trypsin (Shevchenko et al., 1996), cleaned-up with Zip-Tip C18μ (Millipore, Bedford, MA) and analyzed by mass spectrometry using the 4700 Proteomics Analyzer (Applied Biosystems, Foster City, CA). The proteins were identified by the use of mass spectrometry data for the search of primary sequence databases with the MS/MS ion search mode of the Mascot search engine (Matrix Science, Boston, MA).

3. Results

3.1. Embryo culture

Fig. 1A shows a cultured rat embryo at the end of the 24-h culture period. Embryos and yolk sac membranes were separated as samples for 2-DE analysis (Fig. 1B). The amnion and chorio-allantoic placenta were removed and discarded. The size and protein content of the embryos and yolk sac membranes of the cultured rat embryos are shown in Table 1. Protein content in the individual embryo or yolk sac membrane was sufficient for 2-DE anaylsis.

3.2. 2-DE of embryo protein

Proteins of cultured embryos were well separated by 2-DE with the present method (Fig. 2). About 800 protein spots were consistently detected in replicate gels each

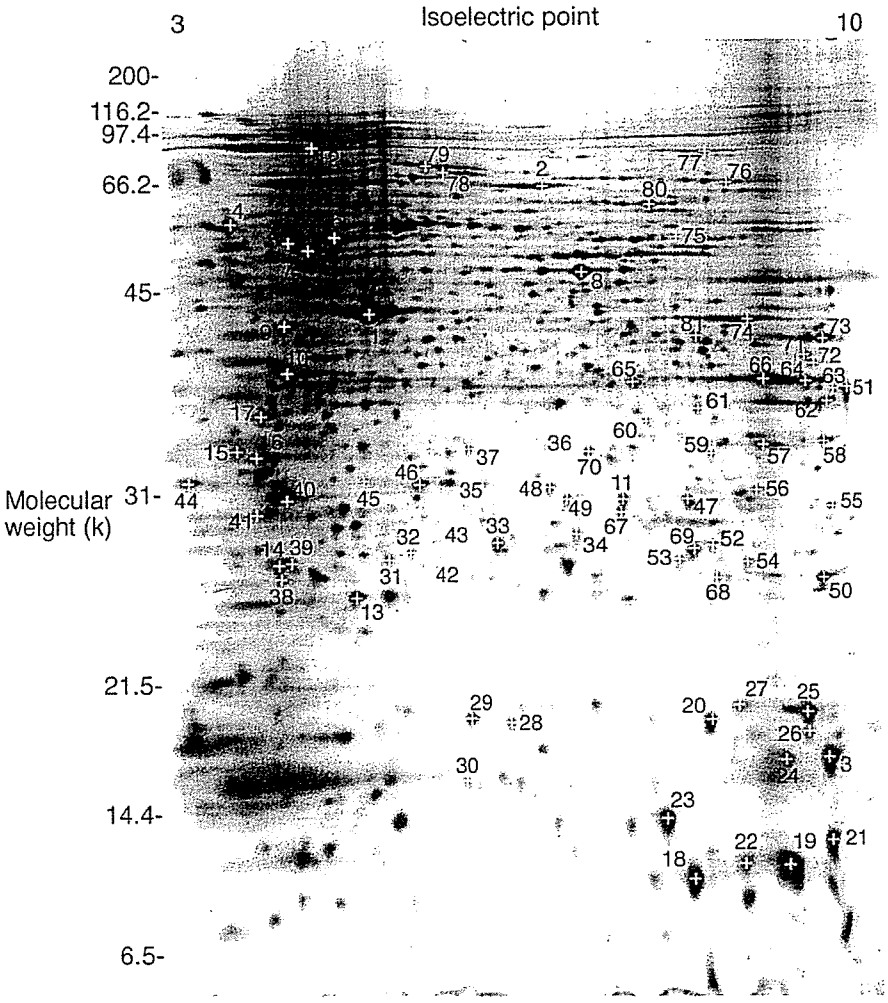

Fig. 2. 2-DE pattern of embryo proteins from a cultured rat embryo equivalent to day 11.5 of gestation. Proteins (50 μg) were separated by IEF with 3–10NL IPG strip (13 cm) and by SDS–PAGE with 12.5% gel (14 × 6 cm), and were stained with silver. Identified protein spots were numbered and listed in Table 2.

Please cite this article in press as: Usami, M. et al., Two-dimensional electrophoresis of protein from cultured postimplantation rat embryos for developmental toxicity studies, Toxicol. In Vitro (2006), doi:10.1016/j.tiv.2006.11.003

Table 2
Protein spots identified in the 2-DE of embryo protein

Spot no.	Accession no.	Protein name	Nominal mass	Calculated pI
1	gi|71620	Actin beta	42,066	5.29
2	gi|19705431	Albumin	70,670	6.09
3	gi|37748460	Peptidylprolyl isomerase A	18,091	8.34
4	gi|11693172	Calreticulin	48,137	4.33
5	gi|202549	Iodothyronine 5′ monodeiodinase	54,375	4.87
6	gi|38014578	Tubulin, beta, 2	50,225	4.79
7	gi|54792127	ATP synthase, H^+ transporting, mitochondrial F1 complex, beta subunit	56,318	5.19
8	gi|38649320	Eno1 protein	51,736	6.70
9	gi|38014840	Laminin receptor 1	32,917	4.80
10	gi|112077	Nucleolar phosphoprotein B23.1	32,711	4.62
11	gi|12844989	Unnamed protein product	28,799	6.67
12	gi|51859516	Heat shock 90 kDa protein 1, beta	83,631	4.97
13	gi|8394432	Peroxiredoxin 2	21,941	5.34
14	gi|6678437	Tumor protein, translationally-controlled 1	19,564	4.76
15	gi|48675371	Complement component 1, q subcomponent binding protein	31,320	4.77
16	gi|34876714	Predicted: similar to Eukaryotic translation elongation factor 1 beta 2	24,831	4.55
17	gi|7242171	Proliferating cell nuclear antigen	29,108	4.66
18	gi|27668426	Predicted: similar to hemoglobin: Subunit = zeta	16,124	6.75
19	gi|3367724	Epsilon 1 globin	16,151	7.90
20	gi|55926145	Expressed in non-metastatic cells 2	17,386	6.92
21	gi|1628436	Profilin	15,149	8.46
22	gi|3367724	Epsilon 1 globin	16,151	7.90
23	gi|40254577	Ribosomal protein S12	14,905	6.81
24	gi|37748460	Peptidylprolyl isomerase A	18,091	8.34
25	gi|509201	Cofilin	18,749	8.22
26	gi|7441446	Destrin	18,661	7.78
27	gi|6671746	Cofilin 2, muscle	18,812	7.66
28	gi|19924089	Expressed in non-metastatic cells 1, protein (NM23A) (nucleoside diphosphate kinase)	17,296	5.96
29	gi|38328242	Stmn1 protein	17,278	5.76
30	gi|12850597	Unnamed protein product	17,138	5.95
31	gi|57006	Unnamed protein product	22,320	5.55
32	gi|202945	Apolipoprotein A-I precursor	30,100	5.52
33	gi|3688521	Thiol-specific antioxidant protein	24,860	5.64
34	gi|8394082	Proteasome (prosome, macropain) subunit, beta type 3	23,235	6.15
35	gi|20071222	NADH dehydrogenase (ubiquinone) Fe-S protein 3	30,358	6.40
36	gi|1381643	Cysteine protease p32-beta	30,097	5.68
37	gi|30410794	Proteasome activator subunit 3 isoform 1	29,602	5.69
38	gi|21312044	Eukaryotic translation initiation factor 3, subunit 12	25,356	4.81
39	gi|6671696	Chromobox homolog 1 (Drosophila HP1 beta)	21,519	4.85
40	gi|27664664	Predicted: similar to 25 kda FK506-binding protein	25,220	9.29
41	gi|6381991	Integrin beta 4 binding protein	27,007	4.63
42	gi|202945	Apolipoprotein A-I precursor	30,100	5.52
43	gi|2897818	Huntingtin interacting protein-2	22,503	5.33
44	gi|6978499	Acidic (leucine-rich) nuclear phosphoprotein 32 family, member A	28,718	3.99
45	gi|47169488	TPA: proteasome subunit alpha type 3-like	28,621	5.19
46	gi|62664759	Predicted: prohibitin	27,757	5.44
47	gi|297111	Phosphoglyceromutase	28,908	8.85
48	gi|16758298	Proteasome (prosome, macropain) subunit, beta type 7	30,250	8.13
49	gi|16758848	Endoplasmic retuclum protein 29	28,614	6.23
50	gi|56789700	Peroxiredoxin 1	22,323	8.27
51	gi|38648863	Malate dehydrogenase, mitochondrial	36,117	8.93
52	gi|16758182	RAN, member RAS oncogene family	24,579	7.01
53	gi|5420030	Glutathione transferase	25,550	6.77
54	gi|25453420	Glutathione S-transferase, pi	23,652	6.89
55	gi|56550075	Proteasome (prosome, macropain) subunit, alpha type 7	28,010	8.60
56	gi|8394069	Proteasome (prosome, macropain) subunit, alpha type 4	29,764	7.59
57	gi|18543331	Guanine nucleotide binding protein, beta polypeptide 2-like 1	35,529	7.60
58	gi|38051979	Vdac1 protein	32,060	8.35
59	gi|1906812	Inducible carbonyl reductase	30,920	7.64
60	gi|62661724	Predicted: similar to esterase D/formylglutathione hydrolase	37,322	6.45

Please cite this article in press as: Usami, M. et al., Two-dimensional electrophoresis of protein from cultured postimplantation rat embryos for developmental toxicity studies, Toxicol. In Vitro (2006), doi:10.1016/j.tiv.2006.11.003

Table 2 (*continued*)

Spot no.	Accession no.	Protein name	Nominal mass	Calculated pI
61	gi|57527447	Ribose-phosphate pyrophosphokinase I -like	35,297	6.51
62	gi|54261548	Lactate dehydrogenase A	36,712	8.45
63	gi|7949053	Heterogeneous nuclear ribonucleoprotein A2/B1 isoform 1	36,028	8.67
64	gi|62653546	Predicted: similar to glyceraldehyde-3-phosphate dehydrogenase	36,045	8.44
65	gi|6978491	Aldehyde reductase 1	36,230	6.26
66	gi|62653546	Predicted: similar to glyceraldehyde-3-phosphate dehydrogenase	36,045	8.44
67	gi|76647405	Predicted: similar to proteasome subunit alpha type 6 (proteasome iota chain) (macropain iota chain)	27,838	6.34
68	gi|8394079	Proteasome (prosome, macropain) subunit, beta type 2	23,069	6.96
69	gi|8394063	Proteasome (prosome, macropain) subunit, alpha type 2	26,024	6.92
70	gi|62655706	Predicted: similar to RIKEN cdna 1110025F24	26,482	5.90
71	gi|61889115	Phosphoserine aminotransferase 1	40,943	7.57
72	gi|66911068	Pcbp2_predicted protein	35,666	8.17
73	gi|202837	Aldolase A	39,691	8.31
74	gi|38649310	Phosphoglycerate kinase 1	44,909	8.02
75	gi|584875	Adenylyl cyclase-associated protein 1 (CAP 1)	51,857	7.16
76	gi|74144333	Unnamed protein product	67,573	7.18
77	gi|19424312	KH-type splicing regulatory protein	74,466	6.38
78	gi|228784	Alpha fetoprotein	70,167	5.71
79	gi|228784	Alpha fetoprotein	70,167	5.71
80	gi|2511703	p60 protein	63,158	6.40
81	gi|2644966	hnRNP-E1 protein	37,987	6.66

Proteins names with their NCBI accession numbers were shown for the protein spots in Fig. 1.

from one embryo. Selected protein spots were analyzed by mass spectrometry and 81 protein spots were identified as shown in Table 2. These protein spots also served as landmarks for the matching of protein spots among the gels.

3.3. 2-DE of yolk sac membrane protein

Proteins of yolk sac membranes were separated as well as those of embryos by 2-DE with the present method (Fig. 3). The 2-DE pattern of yolk sac membranes was fairly different from that of embryos. Most protein spots were common but were quantitatively different between the yolk sac membranes and the embryos. In addition, there were embryo specific and yolk sac membrane specific protein spots.

4. Discussion

The present method is simple and can be carried out concomitantly with in vitro developmental toxicity studies using rat embryo culture. The whole 2-DE procedures are completed within four days. IPG strips with narrower pH ranges would be useful for precise and convenient analysis of specific protein spots. For screening purposes or focused proteomics, the same procedures could be applied to the mini-gel format with shorter IPG strip and mini SDS–PAGE gel.

The primary 2-DE map constructed in the present study is useful for interlaboratory comparison of 2-DE patterns. Abundant and characteristic protein spots can be used as landmarks for matching of the 2-DE pattern. We are planning to identify more protein spots for a more precise and accurate 2-DE map of cultured rat embryos in future, giving priority to protein spots of interest that are differentially expressed due to the effects of developmental toxicants. Identification of very faint protein spots may require a separate 2-DE experiment with an increased amount of applied protein samples.

It is expected that 2-DE analysis by the present method enables informative experiments for developmental toxicity studies. Because protein from less than one embryo is sufficient for 2-DE analysis in the present method, toxic effects observed in individual embryos may be related to the changes in protein expression pattern. Alternatively, analysis of specific parts isolated from single embryos may improve the efficiency of differential analysis. It is also noted that the present method is valid for 2-DE analysis of yolk sac membranes as well as embryos. Simultaneous analysis of yolk sac membranes with embryos would be useful to investigate the action sites of developmental toxicants.

The critical point of the present method is the use of the DeStreak Reagent as an antioxidant and the electrode pads. Both of which greatly improved the 2-DE pattern by decreasing horizontal streaks in the present method. We initially used dithiothreitol or tributylphosphine as a reducing agent to avoid the oxidation of proteins but could not decrease the streaks sufficiently. High concentration of redox agents such as glutathione in the embryo or yolk sac membrane samples (Harris et al., 1995) might affect redox status of proteins when dithiothreitol or tributylphosphine was used.

As far as we tested, addition of protease inhibitors to the lysis/rehydration buffer had no effects on the 2-DE pattern. It is considered that the constituents of the lysis/rehydration buffer were effective for inactivation of proteases in the

Please cite this article in press as: Usami, M. et al., Two-dimensional electrophoresis of protein from cultured postimplantation rat embryos for developmental toxicity studies, Toxicol. In Vitro (2006), doi:10.1016/j.tiv.2006.11.003

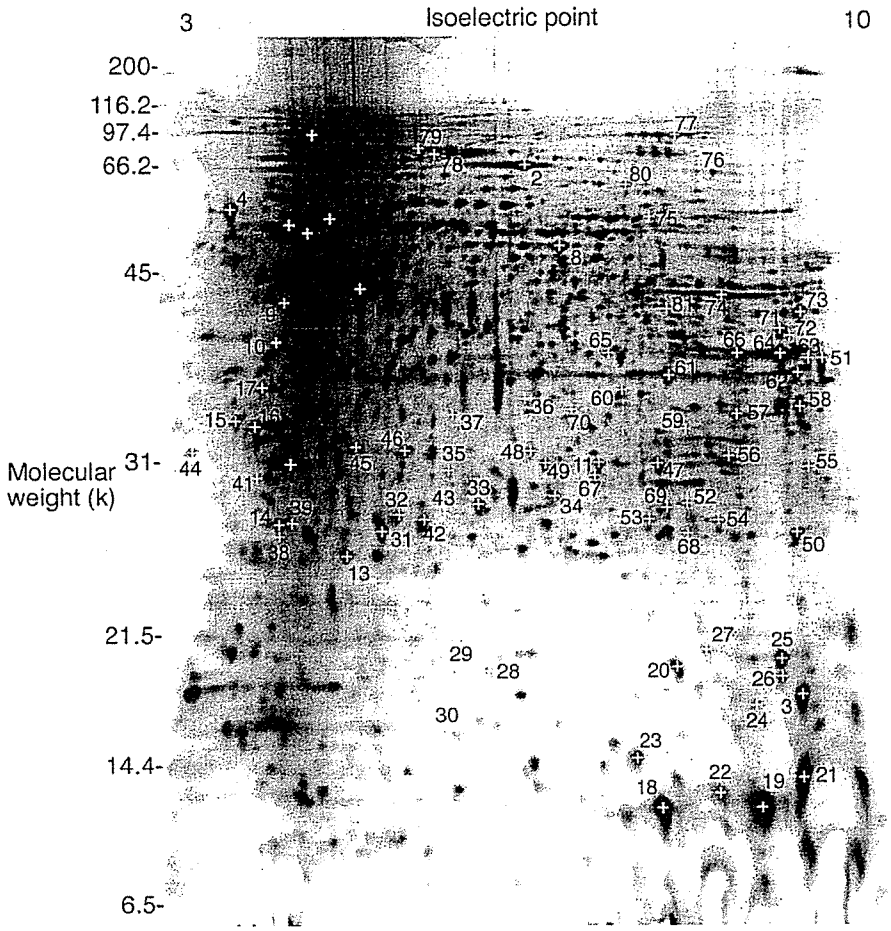

Fig. 3. 2-DE pattern of yolk sac membrane proteins from a cultured rat embryo equivalent to day 11.5 of gestation. Proteins (50 μg) were separated by IEF with 3–10NL IPG strip (13 cm) and by SDS–PAGE with 12.5% gel (14 × 6 cm), and were stained with silver. Proteins identified for the embryo are indicated by the same number as in Fig. 2.

embryo or yolk sac membrane samples. No requirement for protease inhibitors in the present method saves the const and labor in the 2-DE analysis.

In conclusion, it is considered that the present method is suitable for 2-DE analysis of embryos and yolk sac membranes in developmental toxicity studies using postimlantation rat embryo culture.

Acknowledgements

This work was partially supported by the Ministry of Education, Science, Sports and Culture, Grant-in-Aid for Exploratory Research, 15658090, 2003–2005.

References

Baumgartner, B.G., Murach, K.-F., Schlegel, E., Praxmayer, C., Illmensee, K., 1994. Comparison of protein analysis between embryonic and extraembryonic tissues during the 11th day of gestation of the mouse. Electrophoresis 15, 992–1000.

Fountoulakis, M., Berndt, P., Boelsterli, U.A., Crameri, F., Winter, M., Albertini, S., Suter, L., 2000. Two-dimensional database of mouse liver proteins: Changes in hepatic protein levels following treatment with acetaminophen or its nontoxic regioisomer 3-acetamidophenol. Electrophoresis 21, 2148–2161.

Greene, N.D.E., Leung, K.-Y., Wait, R., Begum, S., Dunn, M.J., Copp, A.J., 2002. Differential protein expression at the stage of neural tube closure in the mouse embryo. J. Biol. Chem. 277, 41645–41651.

Harris, C., Hiranruengchok, R., Lee, E., Berberian, R.M., Eurich, G.E., 1995. Glutathione status in chemical embryotoxicity: Synthesis, turnover and adduct formation. Toxicol. in Vitro 9, 623–631.

Laemmli, U.K., 1970. Cleavage of structural proteins during the assembly of the head of bacteriophage T4. Nature 227, 680–685.

Piubelli, C., Cecconi, D., Astner, H., Caldara, F., Tessari, M., Carboni, L., Hamdan, M., Righetti, P.G., Domenici, E., 2005. Proteomic changes in rat serum, polymorphonuclear and mononuclear leukocytes after chronic nicotine administration. Proteomics 5, 1382–1394.

Praxmayer, C., Murach, K.-F., Baumgartner, B., Aberger, F., Schlegel, E., Illmensee, K., 1992. Protein synthesis in murine organs during postimplantation development detected by two-dimensional gel electrophoresis. Electrophoresis 13, 720–722.

Schmid, B., Bechter, R., Kucera, P., 1997. Use of whole emryo cultures in in vitro teratogenicity testing. In: Castell, J.V., Gómez-Lechón, M.J. (Eds.), In Vitro Methods in Pharmacetical Research. Academic Press, San Diego, pp. 353–373.

Shevchenko, A., Wilm, M., Vorm, O., Mann, M., 1996. Mass spectrometric sequencing of proteins from silver-stained polyacrylamide gels. Anal. Chem. 68, 850–858.

Usami, M., Ohno, Y., 1996. Teratogenic effects of selenium compounds on cultured postimplantation rat embryos. Teratog. Carcinog. Mutagen. 16, 27–36.

Xu, H., Hu, L.S., Chang, M., Jing, L., Zhang, X.Y., Li, G.S., 2005. Proteomic analysis of kidney in fluoride-treated rat. Toxicol. Lett. 160, 69–75.

Please cite this article in press as: Usami, M. et al., Two-dimensional electrophoresis of protein from cultured postimplantation rat embryos for developmental toxicity studies, Toxicol. In Vitro (2006), doi:10.1016/j.tiv.2006.11.003

J Artif Organs (200■) ■:■■–■■
DOI 10.1007/s10047-006-0363-y

ORIGINAL ARTICLE

Masato Tamai, PhD · Kazuo Isama
Ryusuke Nakaoka, PhD · Toshie Tsuchiya, PhD

Synthesis of a novel β-tricalcium phosphate/hydroxyapatite biphasic calcium phosphate containing niobium ions and evaluation of its osteogenic properties

Abstract To promote the osteogenic properties of osteoblasts, we synthesized a hydroxyapatite (HAp) with β-tricalcium phosphate (β-TCP) biphasic calcium phosphate containing Nb ions (NbTCP/HAp). NbTCP/HAp was prepared by annealing precipitates obtained by coprecipitation of an aqueous solution of $Ca(NO_3)_2$ and a mixture of $(NH_4)_2HPO_4$ and aqueous Nb solution. The precipitates can be regarded as a calcium-deficient HAp, the PO_4 sites of which are partly occupied by Nb ions. NbTCP/HAp was successfully synthesized by thermal decomposition of the precipitates. NbTCP/HAp enhanced the calcification of normal human osteoblasts (NHOst), and the amount of calcified tissue increased in proportion to the Nb ion concentration in the NbTCP/HAp. The alkaline phosphatase (ALP) activity of NHOst was also enhanced by NbTCP/HAp. Because Nb ions significantly enhance the ALP activity of NHOst, calcification by NbTCP/HAp is considered to be due to enhancement of ALP activity induced by Nb ions dissolved from NbTCP/HAp. These results indicate that NbTCP/HAp can be an effective bone repair material.

Key words Tissue engineering · Bone · Osteoblasts · Calcium phosphate · Nb ions

Introduction

Bone tissue engineering offers a promising alternative strategy for healing severe bone injuries by utilizing the body's natural biological response to tissue damage in conjunction with engineering principles. Osteogenic cells, growth factors, and biomaterial scaffolds form the foundation of the many bone tissue engineering strategies employed to achieve regeneration of damaged bone tissue. An ideal biomaterial scaffold will provide mechanical support to an injured site and also enhance osteogenic differentiation to encourage bone growth.[1] To develop biomaterial scaffolds with optimal performance, understanding the interactions between osteoblasts and scaffolds is extremely important.

Hydroxyapatite [HAp, $Ca_{10}(PO_4)_6(OH)_2$] and related calcium phosphate ceramics, e.g., β-tricalcium phosphate [β-TCP, β-$Ca_3(PO_4)_2$], have good biocompatibility with bone tissue because their chemical compositions are very similar to the mineral phase of human bone. It is well known that these calcium phosphate ceramics can be biologically bonded to natural bone. In fact, it has been reported that porous materials composed of HAp, β-TCP, or β-TCP/HAp biphasic calcium phosphate are useful for bone tissue regeneration because of their osteoconductivity.[2–6] It has also been reported that β-TCP/HAp biphasic calcium phosphate shows better osteoconductivity than HAp or β-TCP alone.[7,8] Therefore, this material has been actively studied for use as a scaffold for bone tissue regeneration.

In a previous study, Nb ions were reported to lower cytotoxicity[9] (IC_{50} of Nb ions for L929 fibroblasts is 3.63×10^3), and we reported that Nb ions significantly promoted the calcification of normal human osteoblasts (NHOst).[10] Furthermore, we succeeded in synthesizing a hydroxyapatite containing Nb ions (NbHAp) and showed that NbHAp has the potential to promote alkaline phosphatase (ALP) activity, an important factor in the generation of new bone, in NHOst.[11] In this study, to further promote the cell activity of osteoblasts, we synthesized β-TCP/HAp biphasic calcium phosphate containing Nb ions and investigated interactions between β-TCP/HAp biphasic calcium phosphate and NHOst in vitro.

Materials and methods

Synthesis and characterization of β-TCP/HAp biphasic calcium phosphate containing Nb ions

Reagent grade $Ca(NO_3)_2$, $(NH_4)_2HPO_4$, and $NbCl_5$ (Wako, Osaka, Japan) were used without purification. NbTCP/HAp

Received: May 26, 2006 / Accepted: September 28, 2006

M. Tamai · K. Isama · R. Nakaoka · T. Tsuchiya
Division of Medical Devices, National Institute of Health Sciences, 1-18-1 Kamiyoga, Setagaya-ku, Tokyo 158-8501, Japan
Tel. +81-3-3700-4842; Fax +81-3-3707-6950
e-mail: ■■

samples were prepared by annealing precipitates obtained from coprecipitation of an aqueous solution of $Ca(NO_3)_2$ with a mixture of $(NH_4)_2HPO_4$ and an aqueous solution of Nb as described below. $Ca(NO_3)_2$ and $(NH_4)_2HPO_4$ were completely dissolved in distilled water. The aqueous Nb solution was prepared by mixing distilled water and $NbCl_5$ dissolved in 5% hydroxyacetone and 5% 2-aminoethanol.[12] A 0.2 M $(NH_4)_2HPO_4$ aqueous solution was combined with 0.01 M $NbCl_5$ and stirred with a magnetic bar at Nb/(Nb + P) molar ratios of 0.0000, 0.0167, or 0.1667. The pH of the mixture was adjusted to 10 using 1 N NaOH throughout the reaction, and 0.2 M $Ca(NO_3)_2$ was slowly dropped into the mixture (20 ml/min). The amount of 0.2 M $Ca(NO_3)_2$ solution was adjusted to a Ca/(Nb + P) molar ratio of 1.6 in order to synthesize β-TCP/HAp biphasic calcium phosphate, followed by stirring the suspension for 24 h at room temperature. The precipitates were centrifuged at 3600 rpm for 5 min and washed with distilled water. The resulting precipitates of Nb/(Nb + P) with molar ratios of 0.0000, 0.0167, and 0.1667 were named NbHAp-0, NbHAp-I, and NbHAp-II, respectively. These precipitates were then annealed at 800°C for 2 h (temperature increase: 5°C/min) and named NbTCP/HAp-0, NbTCP/HAp-I, and NbTCP/HAp-II, respectively. The NbTCP/HAp samples obtained were characterized by X-ray diffraction analysis (XRD, Rint2000, Rigaku, ■■, ■■) with Cu K_α radiation (40 kV, 50 mA). The XRD profiles of 2θ angles between 20° and 60° with a step interval of 0.01° were collected at a scanning rate of 4°/min. Also, measurement of the lattice parameter was carried out using the 211, 112, and 300 planes of HAp, and data for the lattice parameter were collected with a scan rate of 0.025°/min. The observed interplanar spacing was corrected using elemental Si as a standard material.

Concentrations of Ca, P, and Nb ions in the precipitate were estimated by inductively coupled plasma analysis (ICP, HP4500, Hewlett-Packard, ■■, ■■) after the precipitate was dissolved in HNO_3 solution. Microstructural evaluation of the precipitates was performed by scanning electron microscopy (SEM, JSM-5800LV, JEOL, ■■, ■■; acceleration voltage: 25 kV) and energy-dispersive X-ray spectroscopy (EDX) (LV5800, JEOL).

Osteogenic effects of NbTCP/HAp

NbTCP/HAp pellets were fabricated to investigate their effects on the osteogenic function of osteoblasts. In total, 100 mg of powdered NbTCP/HAp was put into a stainless steel mold and uniaxially pressed at 30 MPa for 1 min to form a pellet 0.5 mm in thickness and 12 mm in diameter. The pellets were sintered at 800°C for 2 h (temperature increase: 5°C/min).

NHOst were purchased from BioWhittaker (Walkersville, MD, USA) and maintained in ■■ (αMEM) (Gibco, Grand Island, NY, USA) containing 10% fetal calf serum (FCS, Kokusai Sinyakyu, Tokyo, Japan) in incubators at 37°C in a humid atmosphere with 5% CO_2. All assays were performed using αMEM containing 10% FCS supplemented with 10 mM β-glycerophosphate.

Cells were seeded on the pellets as described below. Each NbTCP/HAp pellet was immersed in 1 ml culture medium in a well of a 24-well cell culture plate (Corning, Corning, NY, USA) and incubated at 37°C for 24 h. After discarding the medium, 300 μl of new culture medium was put into each well, followed by 1 ml of NHOst suspension (4×10^4 cell/ml), and incubation was carried out for 4 h. Finally, the cell-seeded NbTCP/HAp pellet was transferred to a new well of a 24-well plate with 1 ml of the test medium and incubated at 37°C in a humidified atmosphere with 5% CO_2 for 7–14 days.

Extracts from various NbTCP/HAp samples were prepared to investigate their effects on dissolved ions. NbTCP/HAp powder (100 mg/ml) was added to the culture medium (αMEM) containing 10% FCS and immersed at 37°C for 24 h. After changing the medium, the suspensions were stirred by a shaker at 200 rpm for 72 h at 37°C. The suspension was centrifuged at 3600 rpm for 5 min, and the supernatant was collected to use as an extract for an osteogenesis test in vitro. The atomic concentrations of Nb in the extract were measured by ICP.

An NHOst suspension (4×10^4 cells/ml) was added to culture wells and incubated for 4 h. After the NHOst had adhered to the well, the suspension medium was discarded and 1 ml of the extract supplemented with 10 mM β-glycerophosphate was added. The NHOst were incubated at 37°C in a saturated humid atmosphere with 5% CO_2 for 7–14 days.

We also examined the effect of Nb ions on the osteogenesis of NHOst. A solutionn of 0.2 μM $NbCl_5$/αMEM and serial dilutions were prepared. In addition to the experiment using the extracts indicated above, NHOst were cultured in $NbCl_5$/αMEM supplemented with β-glycerophosphate for 7–14 days.

Proliferation of NHOst cells in each experiment was estimated by a TetraColor One assay (Seikagaku, Tokyo, Japan), which incorporates an oxidation–reduction indicator based on detection of metabolic activity. After a 7-day incubation, the culture medium was discarded and 2% TetraColor One/αMEM solution was added to each well and was incubated for 2 h. The absorbance of the supernatant at 450 nm was measured using a μQuant spectrophotometer (Bio-tek, Winooski, VT, USA) to estimate the proliferation of the test cells. After estimating the proliferation, the cells were washed with phosphate-buffered saline [PBS(−)], followed by the addition of 1 ml of 0.1 M glycine buffer (pH 10.5) containing 10 mM $MgCl_2$, 0.1 mM $ZnCl_2$, and 4 mM *p*-nitrophenylphosphate sodium salt. The absorbance of the added buffer at 405 nm after 5 min incubation at room temperature was detected to evaluate the ALP activity of the test cells. After measurement of ALP, the NHOst cultured in the extract were washed with PBS(−) three times and the calcium phosphate deposited by NHOst was estimated. The amount of deposited calcium phosphate dissolved in 0.1 N HCl solution was determined by a Wako Calcium C test kit (Wako), which is based on the *o*-cresolphthalein complex color development method. The NHOst in all assays were stained in 5% Giemsa solution and observed by light microscopy (Nikon, Eclipse TE300, ■■, ■■) to confirm their

Table 1. Chemical composition and characteristics of the precipitates prepared in this study

Sample	Phase	Annealing temperature	Theoretical composition[a]		Measured composition[a]		Color of precipitate	Lattice parameter[b]	
			Ca/(P + Nb)	Nb/(P + Nb)	Ca/(P + Nb)	Nb/(P + Nb)		*a*-axis (nm)	*c*-axis (nm)
NbHAp-0	HAp		1.60	0.000	1.60	–	White	–	–
NbHAp-I	HAp		1.60	0.017	1.56	0.013	Pale yellow	–	–
NbHAp-II	HAp		1.60	0.167	1.56	0.077	Buff yellow	–	–
NbTCPHAp-0	β-TCP + HAp	800°C	1.60	0.000	1.60	–	White	0.939	0.687
NbTCP/HAp-I	β-TCP + HAp	800°C	1.60	0.017	1.56	0.013	White	0.942	0.689
NbTCP/HAp-II	β-TCP + HAp	800°C	1.60	0.167	1.56	0.074	White	0.943	0.690

HAp, hydroxyapatite; NbHAp, hydroxyapatite containing Nb ions; TCP, tricalcium phosphate
[a]Molar ratio
[b]Lattice parameter for HAp

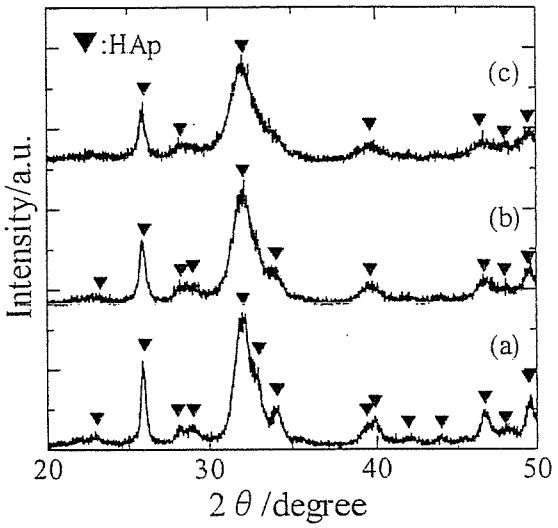

Fig. 1. X-ray diffraction (XRD) patterns of the precipitates with a Ca/(P + Nb) molar ratio of 1.50: *a*, Nb/(Nb + P) = 0; *b*, Nb/(Nb + P) = 0.0167; and *c*, Nb/(Nb + P) = 0.1667. *Triangles* represent XRD peaks due to the crystal structure of hydroxyapatite (HAp)

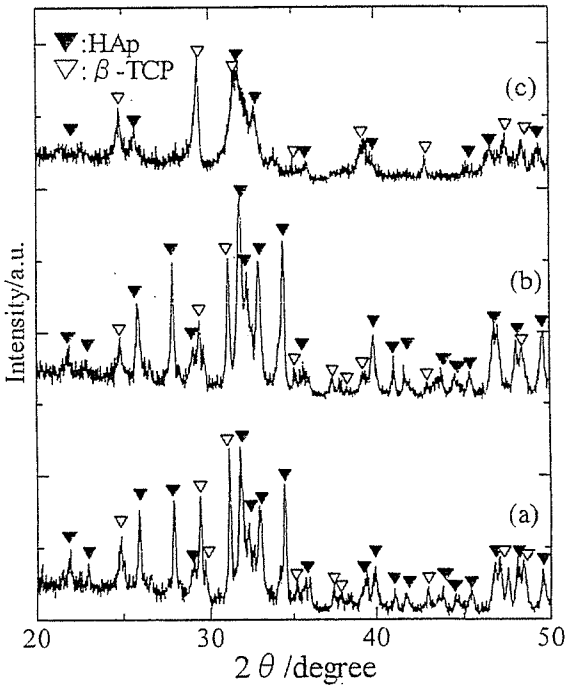

Fig. 2. XRD patterns of the annealed precipitates with a Ca/(P + Nb) molar ratio of 1.50: *a*, Nb/(Nb + P) = 0; *b*, Nb/(Nb + P) = 0.0167; and *c*, Nb/(Nb + P) = 0.1667. These precipitates were annealed at 800°C. *β-TCP*, β-tricalcium phosphate

proliferation. All results were expressed as mean values ± SD and were analyzed statistically with Student's *t* test.

Results

XRD patterns of the precipitates prepared in this study are shown in Fig. 1. The XRD indicated that precipitates with Nb/(Nb + P) molar ratios from 0 to 0.167 had a monolithic apatite structure, irrespective of the Nb/(Nb + P) molar ratio of the starting solution, although the level of crystallite decreased as the Nb content increased. XRD patterns of the precipitates with various Nb/(Nb + P) molar ratios annealed at 800°C are shown in Fig. 2. The level of crystallites of the precipitates was high due to the annealing, and their diffraction peaks were composed of those of both HAp and β-TCP. Interestingly, the crystallite level decreased when the Nb level increased.

The chemical compositions and characteristics of the precipitates prepared in this study are summarized in Table 1. Both the Ca/(Nb + P) and the Nb/(P + Nb) molar ratios in precipitates measured by ICP approximately agreed with their theoretical values, except for the Nb/(P + Nb) molar ratio of NbTCP/HAp-II: the measured Nb/(P + Nb) molar ratio of NbTCP/HAp-II was 0.074, which is lower than the theoretical value of 0.167. The lattice parameter of the HAp phase in NbTCPHAp increased with increasing Nb content.

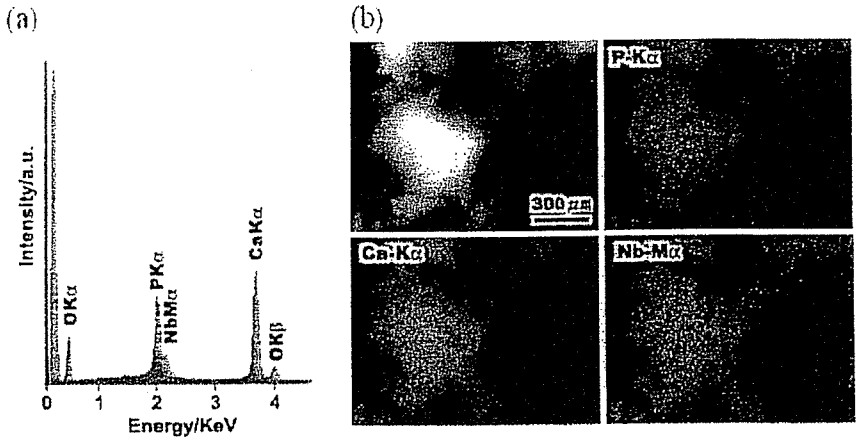

Fig. 3. Scanning electron microscopy–energy-dispersive X-ray spectroscopy spectra of NbTCP/HAp-II annealed at 800°C (a) and their mapping images from P-Kα, Ca-Kα, and Nb-Mα lines (b)

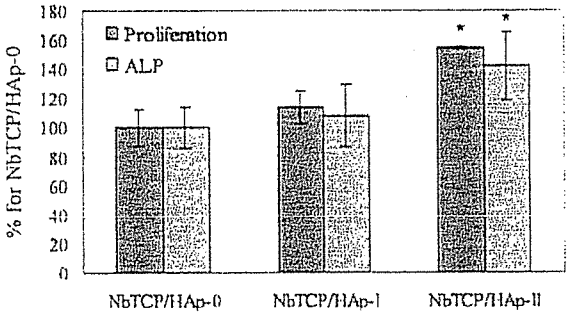

Fig. 4. Proliferation and alkaline phosphatase (*ALP*) activity of normal human osteoblasts (NHOst) cultured on various kinds of NbTCP/HAp pellets. *$P < 0.01$ against NbTCP/HAp-0 (without Nb ions)

The lattice parameters of NbTCP/HAp-0 without Nb ions were 0.939 nm for the *a*-axis and 0.687 nm for the *c*-axis, while those of NbTCP/HAp-II were 0.943 nm for the *a*-axis and 0.690 nm for the *c*-axis. In addition, the color of the precipitates became dark yellow as the Nb/(P + Nb) molar ratio increased, while the annealed precipitates of NbTCP/HAp were white.

SEM observation of the precipitates before annealing revealed that all precipitates were present as aggregates composed of primary particles of less than 1 μm in diameter, irrespective of the Nb/(P + Nb) molar ratio. Figure 3a shows SEM-EDX spectra of NbTCP/HAp-II. The EDX spectrum of Nb Mα was separated from the P K_α line and could be observed at 2.17 KeV, although its intensity was weak. The mapping images of the P-K_α, Ca-K_α, and Nb-M_α lines are shown in Fig. 3b. As shown in Fig. 3b, Nb ions were present at the same site as the Ca and P ions, suggesting that the Nb ions were homogenously distributed in the aggregates.

The proliferation and ALP activity of NHOst cultured on various kinds of NbTCP/HAp pellets is shown in Fig. 4. The proliferation of NHOst cultured on NbTCP/HAp-II pellets was approximately 60% higher than that on NbTCP/HAp-0 without Nb ions ($P < 0.01$). As shown in Fig. 5, many

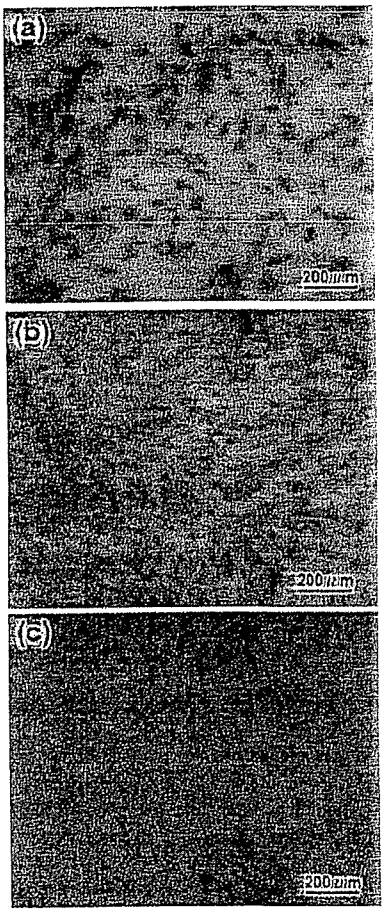

Fig. 5. Light microscopic images of NHOst cultured on various NbTCP/HAp samples for 7 days: *a*, NbTCP/HAp-0; *b*, NbTCP/HAp-I; and *c*, NbTCP/HAp-II. NHOst were stained by Giemsa solution

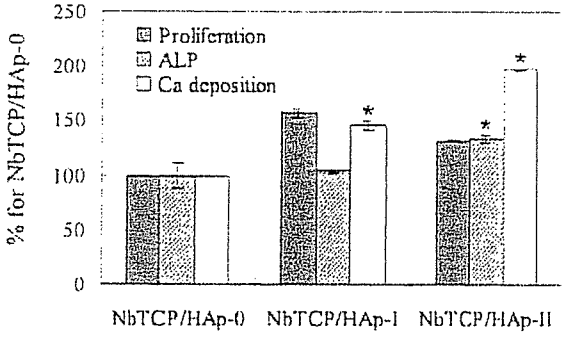

Fig. 6. Osteogenic properties (proliferation, ALP activity, and Ca deposition) of NHOst cultured in extracts from various NbTCP/HAp samples for 14 days. *P < 0.01 against NbTCP/HAp-0 (without Nb ions)

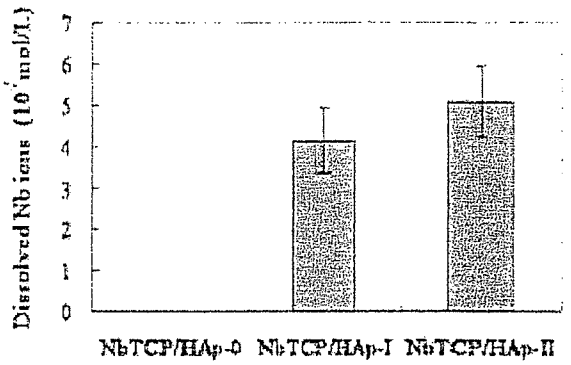

Fig. 7. Concentrations of Nb ions in extracts from various NbTCP/HAp samples. The concentration of Nb ions in cell culture medium was measured by inductively coupled plasma analysis

NHOst adhered to and spread on NbTCP/HAp-I and -II, while little spreading of NHOst was observed on HAp. In addition, as shown in Fig. 4, NHOst cultured on the NbTCP/HAp-II pellets expressed high ALP activity, compared with those cultured on NbTCP/HAp-0. Figure 6 shows the proliferation, ALP activity, and Ca deposition of NHOst cultured in extracts from various NbTCP/HAp samples for 14 days. Like the NHOst cultured on pellets, NHOst cultured in the extract from NbTCP/HAp-II expressed higher ALP activity than those in the extract from NbTCP/HAp-0. Furthermore, the amount of deposited calcium from NHOst increased with increasing Nb ion concentration in NbTCP/HAp, and the calcium deposition in the extract from NbTCP/HAp-II was twice that in the extract from NbTCP/HAp-0.

Figure 7 shows the concentration of Nb ions in extracts from NbTCP/HAp samples. It was found that Nb ions were released into the cell culture medium at concentrations of the order of 1×10^{-5} mol/l. To investigate the effect of Nb ions on NHOst function, NHOst were cultured in a medium containing Nb ions. The dependence of osteogenesis by NHOst on Nb ion concentration is shown in Fig. 8. Nb ions did not affect the proliferation of NHOst, but the ALP activity and Ca deposition of NHOst proceeded proportionally when the concentration of Nb ions was more than 1×10^{-5} mol/L.

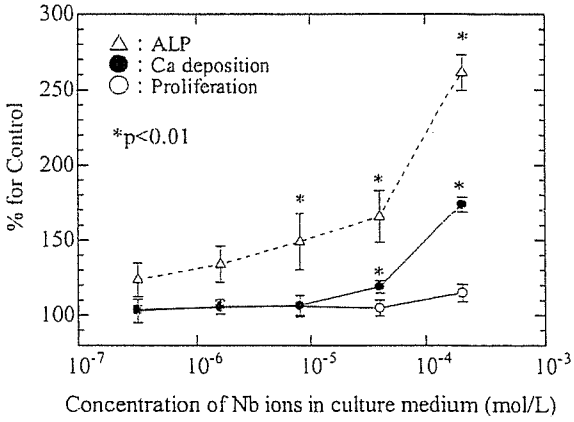

Fig. 8. Relationship between concentration of Nb ions in culture medium and osteogenic properties of NHOst. *P < 0.01 against cell culture medium without Nb ions

Discussion

Characterization of NbTCP/HAp biphasic calcium phosphate ceramics

As summarized in Table 1, before annealing the precipitates, the NbHAp samples were hydroxyapatite with low levels of crystallite. The hydroxyapatite structure is known to be very tolerant of ionic substitution.[12] Ca^{2+} ions, PO_4^{3-} ions, and OH^- ions can be replaced, partly or completely, by various cationic or anionic ions. Notably, as shown in Table 1, the lattice parameter of HAp increased when the Nb content in NbTCP/HAp was high. This fact suggests that Nb ions are taken into the apatite lattice. If a substitution of an Nb^{5+} ion for a Ca^{2+} ion in HAp occurred, the lattice parameter should decrease, since the ionic radius of Ca^{2+} and Nb^{5+} are 0.1 nm and 0.064 nm, respectively. Therefore, the possibility of substitution of Nb ions for Ca ions is low. On the other hand, although the structure of Nb ions in aqueous solution is not fully understood at present, it has been reported that Nb ions in solution are not present as Nb^{5+} but as niobiumate acid, $H_xNb_6O_{19}^{(8-x)-}$ ions (x = 0,1,2) for basic conditions,[14,15] and the niobiumate acid cluster ($H_xNb_6O_{19}^{(8-x)-}$) was polymerized or dissociated depending on the pH and ion concentration.[15] According to these reports, $H_4NbO_6^{3-}$ anionic monomer can exist in basal and low Nb concentrations (<0.08 M). Since the Nb concentration in this study was 0.01 M, Nb ions would exist as $H_4NbO_6^{3-}$ anionic monomers. $H_4NbO_6^{3-}$ may be substituted at the PO_4 site since the PO_4 site in HAp can be replaced by anionic

atomic groups. In addition, the ionic radius of the $H_4NbO_6^{3-}$ monomer and PO_4 are approximately 0.30 nm and 0.23 nm, respectively, suggesting that an increase in lattice parameter of NbTCP/HAp is ascribed to the substitution of PO_4 sites by this monomer in HAp. Furthermore, the fact that both the Ca/(Nb + P) and Nb/(P + Nb) molar ratios of the precipitates, as measured by ICP, approximately agreed with their theoretical values may support this hypothesis. Despite the theoretical Nb/(Nb + P) ratio being 0.1667, the Nb/(Nb + P) molar ratio in NbTCP/HAp-II was about 0.07, which suggests that the maximum amount of substituted Nb ions at the PO_4 site is around 0.07.

The Ca/(P + Nb) molar ratio in the NbHAp obtained in this study was lower than that of the stoichiometric value of 1.67 for HAp. Hydroxyapatite having a lower Ca/P molar ratio is known as calcium-deficient hydroxyapatite [Ca-def HAp, $Ca_{10-Z}(HPO_4)_Z(PO_4)_{6-Z}(OH)_{2-Z}$, Z = 0–1]. Therefore, NbHAp can be regarded as a Ca-def HAp in which the PO_4 sites are partly occupied by Nb ions.

Ca-def HAp decomposes to stoichiometric HAp and β-TCP at temperatures above 600°C according to the following reaction:[16,17]

$$Ca_{10-Z}(HPO_4)_Z(PO_4)_{6-Z}(OH)_{2-Z}\cdot nH_2O \rightarrow (1-Z)Ca_{10}(PO_4)_6(OH)_2 + 3Z\cdot\beta\text{-}Ca_3(PO_4)_2 + Z\cdot nH_2O$$

The above thermal decomposition reaction occurred during the annealing of NbHAp, resulting in a lower Ca/P molar ratio than the stoichiometric value of HAp because of partial β-TCP formation. In addition, the homogenously distributed Nb ions in NbTCP/HAp may result from thermal diffusion of Nb ions during the thermal decomposition process.

Osteogenesis of NHOst cultured on NbTCP/HAp

In this study, NbTCP/HAp showed potential to promote calcification of NHOst. This study indicated that osteogenic behavior of NHOst cultured on NbTCP/HAp pellets was consistent with that of NHOst cultured in extracts from the pellets, suggesting that dissolved ions from the NbTCP/HAp pellets affect calcification of NHOst. As shown in Fig. 7, Nb ions were apparently released from NbTCP/HAps and dissolved in the medium at concentrations of the order of 1×10^{-5} mol/l. When 4×10^{-5} mol/l of $NbCl_5$ was added to the culture medium, Ca deposition clearly increased (Fig. 8). Therefore, the enhancement of Ca deposition is considered to be due to the dissolved Nb ions. One possible mechanism for enhancement of calcification is discussed below.

ALP is known to play an important role in the calcification of bone.[18–20] Generally, the calcification of bone mineral occurs in the matrix vesicles budding from the surface of osteoblasts.[21] The nucleation of biological apatite, which is the initial stage of calcification, occurs due to the reaction between inorganic PO_4^{3-} ions produced by the ALP and calcium ions in matrix vesicles.

NHOst cultured on the NbTCP/HAp pellets containing Nb ions expressed high ALP activity compared with those cultured on HAp without Nb ion. Similarly, it was found that NHOst cultured in an extract from NbTCP/HAp containing Nb ions expressed higher ALP activity than those in the extract from HAp without Nb ions. These results suggest that Nb ions affect the enhancement of ALP activity. Based on the above calcification mechanism in matrix vesicles, the enhancement of calcification might result from the enhancement of ALP activity due to dissolved Nb ions from NbTCP/HAp. The enhancement of ALP activity increases the production of inorganic PO_4^{3-} ions, and then the inorganic PO_4^{3-} ions produced may be taken into the matrix vesicles. The subsequent nucleation of biological hydroxyapatite occurs due to a reaction of Ca ions and inorganic PO_4^{3-} ions, followed by calcification. Although we cannot deny that Nb ions directly promote calcification by NHOst unrelated with ALP expression, the essence of the calcification enhancement by NbTCP/HAp may be the enhancement of ALP activity by Nb ions dissolved from NbTCP/HAp. The biological effect of Nb ions on NHOst is under investigation. Although further studies are necessary to clarify the mechanism of enhanced calcification by Nb ions, this study strongly suggests that NbTCP/HAp is a more promising material for use as a bone tissue engineering scaffold than HAp.

Conclusion

In order to promote the osteogenicity of osteoblasts, we synthesized a combination of HAp and β-TCP biphasic calcium phosphate containing Nb ions (NbTCP/HAp). The NbTCP/HAp samples were prepared by annealing precipitates obtained by coprecipitation of an aqueous solution of $Ca(NO_3)_2$ with a mixture of $(NH_4)_2HPO_4$ and aqueous Nb solution. The precipitates obtained by the coprecipitation process can be identified as Ca-def HAp, the PO_4 sites of which are partly occupied by Nb ions. NbTCP/HAp samples were successfully obtained by thermal decomposition of the precipitates.

NbTCP/HAp enhanced calcification of NHOst. The enhancement of calcification of NbTCP/HAp was ascribed to the enhancement of ALP activity due to the dissolved Nb ions from NbTCP/HAp.

Acknowledgments This study was supported in part by a Grant-in-Aid for Scientific Research on Advanced Medical Technology from the Ministry of Labour, Health and Welfare of Japan, and a Grant-in-Aid from the Japan Health Sciences Foundation.

References

1. Service FR. Tissue engineers build new bone. Science 2000;289: 1498–1500
2. Tamai N, Myoui A, Tomita T, Nakase T, Tanaka J, Ochi T, Yoshikawa H. Novel hydroxyapatite ceramics with an interconnective porous structure exhibit superior osteoconduction in vivo. J Biomed Mater Res 2002;59:110–117
3. Ohgushi H, Goldberg VM, Caplan IA. Heterotopic osteogenesis in porous ceramics induced by marrow cells. J Orthop Res 1989;7: 568–578

4. Cheung SH, Haak HM. Growth of osteoblasts on porous calcium phosphate ceramic: an in vitro model for biocompatibility study. Biomaterials 1989;10:63–67
5. Uchida A, Nade S, McCartney E, Ching W. Growth of bone marrow cells on porous ceramics in vitro. J Biomed Mater Res 1987;21:1–10
6. Ohgushi H, Okumura M. Osteogenic capacity of rat and human marrow cells in porous ceramics. Acta Orthop Scand 1990;61: 431–434
7. Schopper C, Ziya-Ghazvini F, Goriwoda W, Moser D, Wanschitz F, Spassova E, Lagogiannis G, Auterith A, Ewers R. HA/TCP compounding of a porous CaP biomaterial improves bone formation and scaffold degradation – a long term histological study. J Biomed Mater Res B 2005;74B:458–467
8. Yuan H, Van DDM, Shihong L, Groot BV, Bruijn DDJ. A comparison of the osteoinductive potential of two calcium phosphate ceramics implanted intramuscularly in goats. J Mater Sci Mater Med 2002;13:1271–1275
9. Yamamoto A, Honma R, Sumita M. Cytotoxicity evaluation of 43 metal salts using murine fibroblast and osteoblastic cells. J Biomed Mater Res 1998;39:331–340
10. Isama K, Tsuchiya T. ■■ Bull Natl Inst Health Sci 2003;121:111
11. Tamai M, Nakaoka R, Isama K, Tsuchiya T. Novel calcium phosphate ceramics: the remarkable promoting action on the differentiation of normal human osteoblasts. Key Eng Mater 2006; 309–311:97–100
12. Ohya T, Ban T, Ohya Y, Takahashi Y. Preparation of concentrated, halogen-free aqueous titanium solution. Ceram Trans 2001;112: 47–52
13. Elliott CJ. Structure and chemistry of the apatites and other calcium orthophosphates. Tokyo: Elsevier, 1994
14. Cotton AF, Wilkinson G. Advanced inorganic chemistry. Tokyo: Baifukan, 1994
15. Jehng JM, Wachs IE. Niobium oxide solution chemistry. J Raman Spec 1991;22:83–89
16. Tamai M, Nakamura M, Isshiki T, Nishio K, Endoh H, Nakahira A. A metastable phase in thermal decomposition process of Ca-deficient hydroxyapatite. J Mater Sci Mater Med 2003;14: 617–622
17. Gibson IR, Rehman I, Best SM, Bonfield W. Characterization of the transformation from calcium-deficient apatite to beta-tricalcium phosphate. J Mater Sci Mater Med 2000;11:533–539
18. Genge RB, Sauer RG, Wu YLN, McLean MF, Wuthier ER. Correlation between loss of alkaline phosphatase activity and accumulation of calcium during matrix vesicle-mediated mineralization. J Biol Chem 1988;263:18513–18519
19. Sowa H, Kaji H, Yamaguchi T, Sugimoto T, Chihara K. Smad3 promotes alkaline phosphatase activity and mineralization of osteoblastic MC3T-E1 cells. J Bone Miner Res 2002;17: 1190–1199
20. Wennberg C, Hessle L, Lundberg P, Mauro S, Narisawa S, Lerner HU, Millan LJ. Functional characterization of osteoblasts and osteoclasts from alkaline phosphatase knockout mice. J Bone Miner Res 2000;15:1879–1888
21. Anderson CH. Molecular biology of matrix vesicles. Clin Orthop 1995;314:266–280

J_ID: ZA1 Customer A_ID: 30931 Cadmus Art: JBMA1519 Date: 3-AUGUST-06 Stage: I Page: 1

Markedly different effects of hyaluronic acid and chondroitin sulfate-A on the differentiation of human articular chondrocytes in micromass and 3D honeycomb rotation cultures

Nasreen Banu, Toshie Tsuchiya
Division of Medical Devices, National Institute of Health Sciences, 1-18-1, Kamiyoga, Setagaya-ku, Tokyo 158-8501, Japan

Received 20 September 2005; revised 19 April 2006; accepted 22 May 2006
Published online 00 Month 2006 in Wiley InterScience (www.interscience.wiley.com). DOI: 10.1002/jbm.a.30931

Abstract: A source of morphologically and functionally available human cartilagenous tissue for implantation is required in the field of tissue engineering. To achieve this goal, we evaluated the effects of hyaluronic acid (HA-810 and 1680 kDa), and chondroitin sulfate (CS-A 16 and C-34 kDa) on human articular chondrocytes (HC) in micromass and rotation culture conditions. Cell proliferation was increased by CS-A 16 kDa under micromass and rotation cultures, while cell differentiation was increased under rotation but not micromass conditions. Proliferation and differentiation due to CS-C 34 kDa were very similar to the control under both culture conditions. With HA, cell proliferation was increased depending on the molecular weight under micromass and rotation conditions. In contrast, chondrocyte differentiation was enhanced under rotation conditions, but decreased under micromass conditions depending on the molecular weight of HA. In both culture conditions, aggrecan gene was continuously expressed. However, the collagen type II gene was more weakly expressed in rotation than the micromass culture conditions. Thus, the chemical structures of polysaccharides, and the culture condition, rotation or micromass, caused differences in chondrogenesis. © 2006 Wiley Periodicals, Inc. J Biomed Mater Res 79A: 000–000, 2006

Key words: human articular cartilage; hyaluronic acid; chondroitin sulfate; chondrogenesis; *in vitro* culture

INTRODUCTION

The limited potential of human hyaline cartilage for self-renewal has encouraged research in autologous chondrocyte transplantation for the regeneration of hyaline cartilage following traumatic cartilage damage.[1,2] The development of bioengineered cartilaginous implants is being studied in the field of tissue engineering. A primary approach in tissue engineering involves the regeneration of tissue by growing isolated chondrocytes on polymorphic scaffolds to produce a three-dimensional articular cartilage tissue suitable for implantation.[3–5] Cell seeded scaffolds were tested in the *in vitro* engineering of three-dimensional (3D) hyaline cartilage, although production of hyaline cartilage remains a challenge. Different nonbiodegradable materials tested for cartilage tissue repair in different experimental animals include polytetrafluoroethylene (PTFE),[6] polyethylene terephthalate (Dacron),[7,8] polyurethanes,[9] polyhydroxyethyl methacrylate (PHEMA),[10] polyvinyl alcohol (PVA, Ivalon™),[11] and a variety of other hydrogels.[12,13] Many studies have evaluated the potential of various natural bioabsorbable polymers such as collagen,[14,15] alginates,[16–18] fibrin,[19–21] and gelatin.[22] In recent years, extensive experiments have been performed that support the growth of chondrocytes by using various synthetic bioabsorbable materials in animal models to facilitate the regeneration of cartilage tissue.[23–27]

Hyaluronic acid (HA) is a negatively charged glycosaminoglycan (GAG) composed of repeated disaccharides of D-glucuronic acid and *N*-acetyl-D-glucosamine monomers that is considered the "backbone" of the extracellular ground substance. By interacting with other matrix molecules, HA provides stability and elasticity to the extracellular matrix[28–31] Among many biochemical regulators of articular cartilage, HA of animal origin plays an important role in maintaining the articular chondrocyte morphology and proliferation[32] and

Correspondence to: T. Tsuchiya Ph.D.; e-mail: tsuchiya@nihs.go.jp
Contract grant sponsor: Health and Labour Sciences Research
Contract grant sponsor: Research on Advanced Medical Technology, Ministry of Health, Labour and Welfare and Japan Health Sciences Foundation